Cycloaddition | *Hot Paper*

Tailoring Magnetic Features in Zigzag-Edged Nanographenes by Controlled Diels–Alder Reactions

M. R. Ajayakumar,*[a] Yubin Fu,[a] Fupin Liu,[b] Hartmut Komber,[c] Valeriya Tkachova,[a] Chi Xu,[d] Shengqiang Zhou,[d] Alexey A. Popov,[b] Junzhi Liu,*[e] and Xinliang Feng*[a]

Abstract: Nanographenes (NGs) with tunable electronic and magnetic properties have attracted enormous attention in the realm of carbon-based nanoelectronics. In particular, NGs with biradical character at the ground state are promising building units for molecular spintronics. However, most of the biradicaloids are susceptible to oxidation under ambient conditions and photolytic degradation, which hamper their further applications. Herein, we demonstrated the feasibility of tuning the magnetic properties of zigzag-edged NGs in order to enhance their stability via the controlled Diels–Alder reactions of *peri*-tetracene (**4-PA**). The unstable **4-PA** ($y_0 = 0.72$; half-life, $t_{1/2} = 3$ h) was transformed into the unprecedented benzo-*peri*-tetracenes (**BPTs**) by a one-side Diels–Alder reaction, which featured a biradical character at the ground state ($y_0 = 0.60$) and exhibited remarkable stability under ambient conditions for several months. In addition, the fully zigzag-edged circumanthracenes (**CAs**) were achieved by two-fold or stepwise Diels–Alder reactions of **4-PA**, in which the magnetic properties could be controlled by employing the corresponding dienophiles. Our work reported herein opens avenues for the synthesis of novel zigzag-edged NGs with tailor-made magnetic properties.

Introduction

Nanographenes (NGs)[1–5] have attracted increasing attention due to their intriguing electronic and optical properties, which render them as potential materials in carbon-based nanoelectronics.[6,7] Particularly, NGs can serve as molecular model for understanding the structure-property relationship of the infinite graphene and graphene nanoribbons (GNRs).[8–10] Bottom-up organic synthesis is an indispensable tool to fabricate atomically precise NGs with well-defined electronic structures. In the last decade, NGs with open-shell biradical character at the ground state[11–19] have emerged as promising candidates for molecular spintronics and nonlinear optics,[20–24] nonetheless, their poor chemical stability[25–27] essentially hampered their further applications. For instance, *peri*-tetracene (**4-PA**),[28–30] an open-shell *peri*-acene (the biradical character, $y_0 = 0.72$)[31] with rich zigzag edges (Scheme 1 a), was recently accomplished through the solution-based synthesis by our group and others. However, **4-PA** is highly unstable under ambient condition (half-life, $t_{1/2} = 3$ h), making it difficult for electronic and spintronic applications. Accordingly, effective synthetic strategies are required towards the synthesis of highly stable zigzag-edged NGs with an open-shell character.

Herein, we report the synthesis of zigzag-edged NGs with tailor-made magnetic properties through the controlled Diels–Alder reactions[32–34] of **4-PA** with suitable dienophiles (Scheme 1 b). The unprecedented benzo-*peri*-tetracenes (**BPTs**)[35,36] possessed moderate open-shell biradical characters whereas the circumanthracenes (**CAs**)[28,37,38] exhibited closed-shell or open-shell features depending on the dienophile employed. Among them, the open-shell **BPTs** (**BPT 1**, $y_0 = 0.55$; **BPT 2**, $y_0 = 0.61$) were synthesized (yields: 40% for **BPT 1** and 20% for **BPT 2**) by one-side Diels–Alder reactions of **4-PA** with *p*-chloranil (**1**) and 2,3-dichloro-5,6-dicyano-1,4-benzoquinone (DDQ, **2**), respectively (Scheme 1 b, *route i*). **BPT 1** was able to execute further Diels–Alder reaction by virtue of its reactive

[a] Dr. M. R. Ajayakumar, Y. Fu, Dr. V. Tkachova, Prof. Dr. X. Feng
Center for Advancing Electronics Dresden (cfaed) &
Faculty of Chemistry and Food Chemistry, Technische Universität Dresden
Mommsenstrasse 4, 01062 Dresden (Germany)
E-mail: ajayakumar.murugan_rathamony@tu-dresden.de
xinliang.feng@tu-dresden.de

[b] Dr. F. Liu, Dr. A. A. Popov
Leibniz Institute for Solid State and Materials Research
Helmholtzstraße 20, 01069 Dresden (Germany)

[c] Dr. H. Komber
Leibniz-Institut für Polymerforschung Dresden e. V.
Hohe Straße 6, 01069 Dresden (Germany)

[d] C. Xu, Dr. S. Zhou
Helmholtz-Zentrum Dresden-Rossendorf
Institute of Ion Beam Physics and Materials Research
Bautzner Landstrasse 400, Dresden 01328 (Germany)

[e] Dr. J. Liu
Department of Chemistry and State Key Laboratory of Synthetic Chemistry
The University of Hong Kong
Pokfulam Road, 999077 Hong Kong (P. R. China)
E-mail: juliu@hku.hk

Supporting information and the ORCID identification number(s) for the author(s) of this article can be found under: https://doi.org/10.1002/chem.202001130.

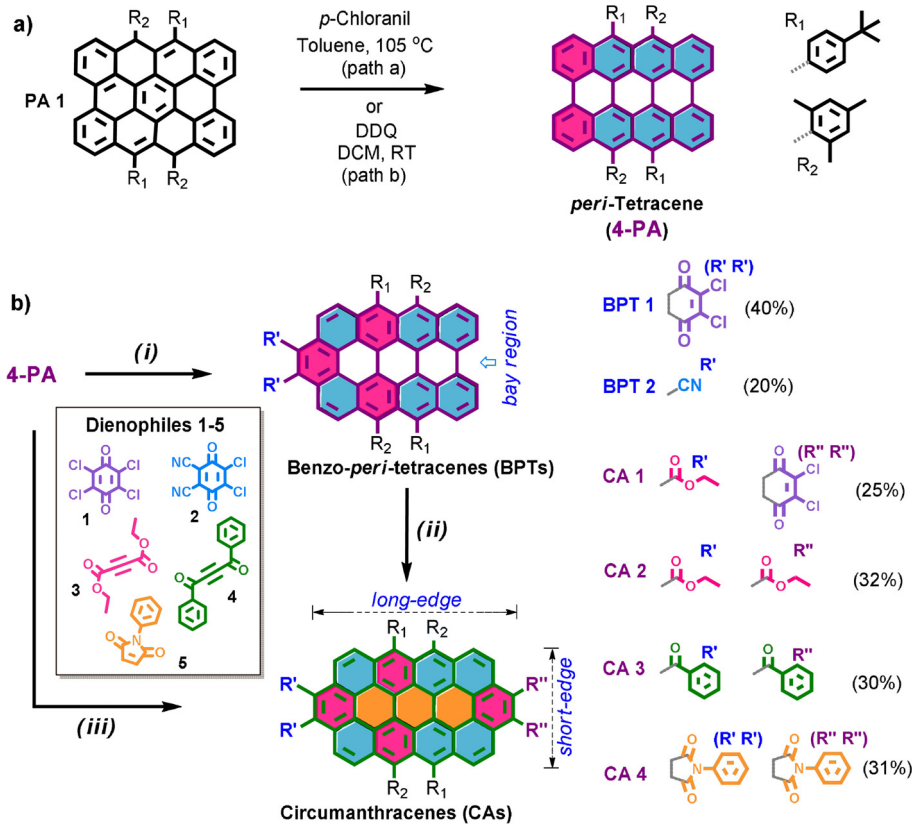

Scheme 1. a) Synthesis of *peri*-tetracene (**4-PA**) from **PA 1** by using *p*-chloranil (path a) or DDQ (path b). b) Synthesis of open-shell **BPT 1**–**2**, open-shell **CA 1** and closed-shell **CA 2**–**4**, via controlled Diels–Alder reactions (**BPT 1**–**2** via *i*: Diels–Alder reaction of **4-PA** with **1** and **2**, respectively, and the successive aromatization; **CA 1** via *ii*: Diels–Alder reaction of **BPT 1** with **3** and the successive aromatization; **CA 2**–**4** via *iii*: Diels–Alder reaction of **4-PA** with **3**, **4** and **5**, respectively, and the successive aromatization).

bay region to afford open-shell **CA 1** ($y_0 = 0.46$) in 25% yield (Scheme 1b, *route ii*). Furthermore, two-side Diels–Alder reactions of **4-PA** with dienophiles, such as diethyl acetylenedicarboxylate (**3**), 1,4-diphenyl-2-butyne-1,4-dione (**4**) and *N*-phenylmaleimide (**5**), provided closed-shell **CA 2**, **CA 3** and **CA 4** (Scheme 1b, *route iii*), respectively, in moderate yields (≈30%). The optical and electrochemical energy-gaps are estimated to be 1.1–1.5 eV for the open-shell **BPT 1**, **BPT 2** and **CA 1**, among them, **BPT 1** possesses the narrowest energy-gap (1.1 eV). Moreover, the magnetic properties of the open-shell **BPT 1**, **BPT 2** and **CA 1** were analyzed by electron paramagnetic resonance (EPR) and superconducting quantum interfering device (SQUID) measurements, as well as supported by the theoretical calculations. Importantly, all these open-shell **BPT 1**, **BPT 2** and **CA 1** displayed high air-stability, and there was no noticeable degradation over one month under ambient conditions. Our work demonstrated herein paves the way for the rational synthesis of open-shell zigzag-edged NGs with remarkable stability and tailor-made magnetic properties.

Results and Discussion

The synthetic procedure is based on the key precursor **PA 1**,[28] which can readily yield **4-PA** through dehydrogenation with *p*-chloranil or DDQ (Scheme 1a). First, **PA 1** was oxidized into **4-PA** in the presence of *p*-chloranil at 105 °C in toluene (Scheme 1a, path a), which further underwent Diels–Alder cycloaddition with the additional *p*-chloranil in the reaction mixture (Scheme 1b, *route i*).[39] The aromatization of the resultant Diels–Alder adduct (a plausible mechanism of the Diels–Alder reaction was proposed in Scheme S1) occurred by the elimination of two HCl molecules and afforded **BPT 1** (along with the inseparable monochloro derivative as minor impurity, Scheme S1) in 40% yield. However, the large excess of *p*-chloranil did not prompt two-fold Diels–Alder reaction of **4-PA**, instead it led to undesired chlorination of the **BPT** core (Scheme S1 and Figure S11). Furthermore, a slow addition of 2 equiv DDQ into the dichloromethane (DCM) solution of **PA 1** at room temperature was carried out. The in situ generated **4-PA** executed Diels–Alder reaction with the DDQ (Scheme S2),[28,40,41] and afforded **BPT 2** as dark-brown solid (20% yield). Interestingly, further treatment of **BPT 1** with diethyl acetylenedicarboxylate (**3**) dienophile at 105 °C in toluene and followed addition of excess *p*-chloranil into the mixture gave **CA 1** in 25% yield (Scheme 1b, *route ii*), in which the short-edges (Scheme S3) of the CA core were asymmetrically installed with the carboxylic esters and dichloro-*p*-benzoquinone. Regarding the synthesis of **CA 2**, **CA 3** and **CA 4**, two-fold Diels–Alder cycloadditions of **4-PA** with various dienophiles were performed (Scheme 1b, *route iii*). The precursor **PA**

1 in dry toluene was treated with 2.5 equiv of *p*-chloranil in presence of excess dienophile **3** at 105 °C to afford **4-PA**. The in situ formed **4-PA** underwent two-fold Diels–Alder reaction with **3**, and the successive aromatization of the adduct (Scheme S4) yielded **CA 2** (32%) as dark green powder. Following the similar synthetic strategy, **CA 3** (30%) and **CA 4** (31%) were achieved using dienophiles **4** and **5**, respectively. All of the **BPTs** and **CAs** were fully characterized by high-resolution MALDI-TOF mass spectrometry and NMR (^{1}H, ^{13}C and 2D) spectroscopy (see the Supporting Information).

Single crystals suitable for X-ray analysis were grown by slow diffusion of methanol into chloroform solution of **CA 2** and **CA 3**. X-ray crystallographic analyses of **CA 2** and **CA 3** reveal that the CA cores are slightly non-planar due to the presence of zigzag-edge substituents (Figure 1).The planes of

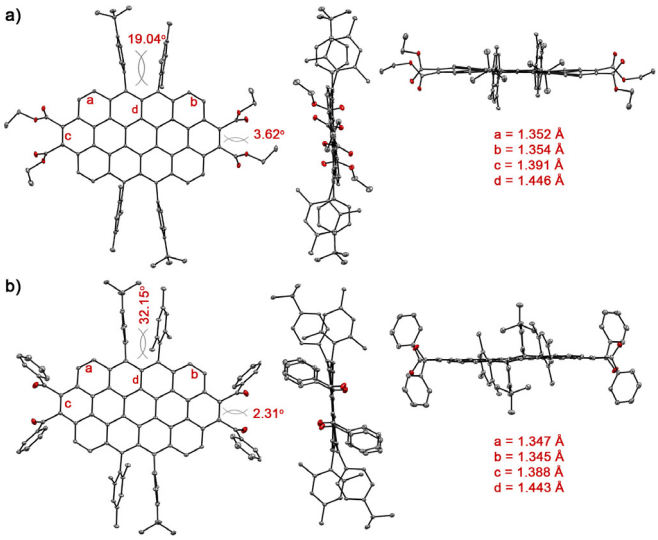

Figure 1. X-ray crystallographic molecular structures of a) **CA 2** and b) **CA 3** (top and side views). Hydrogen atoms and solvent molecules are omitted for clarity. Ellipsoids are drawn at 30% probability level.

the *tert*-butylphenyl and mesityl groups are nearly parallel to each other, whereas perpendicular to the plane of the respective CA cores. The torsional angles between the *tert-butyl*phenyl groups and mesityl groups are measured as 19.04° and 32.15° for **CA 2** and **CA 3**, respectively. The C–C bond lengths at the *peri*-positions (*a, b*) of **CA 2** and **CA 3** are the shortest (≈1.35 Å) in contrast to the other C–C bonds of the CA motif, and hence both of them show the strongest double bond character. The unusual lengthening of the d bond (1.44 Å) is attributed to the steric effect of the bulk phenyl substituents at the zigzag edge periphery.[28]

Next, the magnetic properties of open-shell compounds **BPT 1**, **BPT 2** and **CA 1** were investigated by electron paramagnetic resonance (EPR) and superconducting quantum interfering device (SQUID) measurements (Figure 2). The solid samples of **BPT 1**, **BPT 2** and **CA 1** showed intense EPR signals at room temperature (Figure 2 inset). The broad unresolved signals of **BPT 1**, **BPT 2** and **CA 1** gave *g* values of 2.0026, 2.0031 and

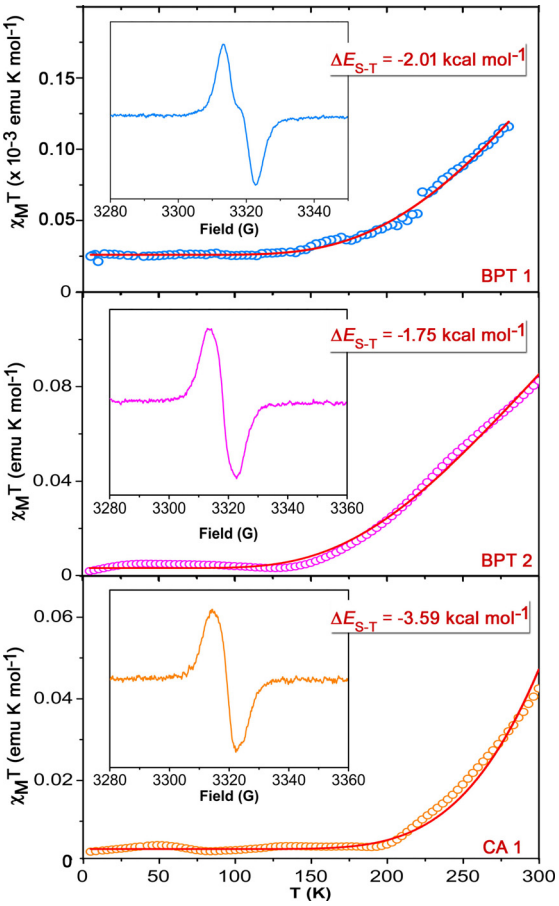

Figure 2. SQUID measurements of powder samples of **BPT 1** (along with the monochloro **BPT 1** impurity), **BPT 2** and **CA 1**. The inset figures show the respective EPR measurements at room temperature. The solid lines are fitted by the Bleaney–Bowers equation.

2.0029, respectively.[27] The line widths were 9.45, 9.03 and 7.98 G for **BPT 1, BPT 2** and **CA 1**, respectively. Furthermore, temperature-dependent SQUID measurements (in the range of 4–300 K) were conducted with the powder samples of **BPT 1**, **BPT 2** and **CA 1**. The samples were cooled down to 4 K without external magnetic field then the data was collected during heating to 300 K under an applied magnetic field of 1 T. Plots of the product of molar magnetic susceptibility (χ_M) with the temperature (*T*) revealed a continuous increase after 150–200 K.

For a further investigation, the data of $\chi_M T$ vs. *T* were fitted by using Bleaney–Bowers equation [Eq. (1)]:[42]

$$\chi_M T = \frac{N_A \mu_B^2 g^2}{k_B} \frac{[2\exp(\frac{2J}{k_B T})]}{1 + 3\exp(\frac{2J}{k_B T})}$$

in which N_A is the Avogadro number, μ_B is the Bohr magneton, $g = 2.0$ is the *g*-factor, k_B is the Boltzmann constant, and *J* is the total angular momentum quantum number. Accordingly, the singlet-triplet energy gap ($\Delta E_{S\text{-}T} = -2J/k_B T$) were found to be −2.01, −1.75 and −3.59 kcal mol^{-1} for **BPT 1**, **BPT 2** and **CA 1**, respectively. All these experimental results confirm that **BPT**

1, **BPT 2** and **CA 1** display a singlet open-shell ground state. Variable-temperature ^{1}H NMR measurements show no significant signal broadening caused by an increasing population of the paramagnetic triplet state at higher temperatures (Figures S13, S22, S29). Slowed-down motion of the quinoid ring in **BPT 1** and **CA 1** probably causes the line broadening and upfield shift that are observed at lower temperatures for protons adjacent to this moiety (Figures S14, S29).

To gain further insights into the electronic structures of **BPT 1**, **BPT 2** and **CA 1**, Hartree–Fock (HF) and DFT calculations were performed. The biradical index (y_0), that reflects the degree of biradical feature, was calculated by symmetry-broken UHF/6-31G* method based on natural orbital (NO) occupations.[31] Owing to the gain of additional Clar's sextets[4,38] and thereby the increase in aromatic stabilization energies (Scheme S5), the open-shell characters are decreased from **4-PA** to **BPTs**/**CAs**. In the case of **CA 1**, the CA core is laterally π-extended with a quinoid ring (Scheme S6) and, hence, the energy-gap (ΔE_g) is lowered (1.3 eV) compared to that of **CA 2**–**4** ($\Delta E_g \approx 1.8$ eV).[38] Thus, the evolution of moderate biradical feature in **CA 1** is justified. Additionally, the singly occupied molecular orbitals (SOMOs α and β) and anisotropy of the induced current-density (ACID)[43] maps of **BPT 1**, **BPT 2**, and **CA 1** calculated at UB3LYP/6-31G(d,p) level indicate that the electron densities are distributed over their aromatic core, whereas the electron densities are more localized over the zigzag periphery in **4-PA** (Figure S50–S52). Therefore, it is supported that, upon benzannulation of the bay position of **4-PA**, the electron density would extend to the newly fused benzene moieties. The calculated singlet biradical indices (y_0) are 0.55, 0.61 and 0.46, for **BPT 1**, **BPT 2** and **CA 1**, respectively, which are noticeably smaller than **4-PA** ($y_0 = 0.72$). Moreover, the **BPT** and **CA** core of these molecules possess clock-wise electronic current flow, thus indicating their global aromaticity.

The UV/Vis-NIR and fluorescence spectroscopies of **BPTs** and **CAs** were performed (**BPT 1**, **BPT 2**, **CA 2** and **CA 3** in CH_2Cl_2; **CA 1** and **CA 4** in $C_2H_2Cl_4$). As shown in Figure 3a, **BPT 1** displayed broad absorption at NIR region, which are centered at 809 nm ($\varepsilon = 24700\ M^{-1}cm^{-1}$) and 920 nm ($\varepsilon = 10800\ M^{-1}cm^{-1}$), whereas **BPT 2** revealed intense absorption with a maximum at 788 nm ($\varepsilon = 59500\ M^{-1}cm^{-1}$). **CA 1** showed broad NIR absorption band with a maximum at 816 nm ($\varepsilon = 17900\ M^{-1}cm^{-1}$). The NIR absorptions (750–1100 nm) of **BPT 1**, **BPT 2** and **CA 1** can be attributed to their open-shell biradical characters at the ground state.[19,35] The time-dependent UV/Vis-NIR measurements of **BPT 1**, **BPT 2** and **CA 1** were conducted under ambient conditions to investigate their kinetic stabilities. During the measurement, the solutions of **BPT 1**, **BPT 2** and **CA 1** were exposed to ambient air and sun light conditions (Figure S1–S3). There was no significant change of the intensities of the absorption spectra of **BPT 1**, **BPT 2** and **CA 1** with the time. All these results support the air stability of **BPT 1**, **BPT 2** and **CA 1**. In contrast, compounds **CA 2**, **CA 3** and **CA 4** displayed sharp absorptions at 630 nm ($\varepsilon = 71300\ M^{-1}cm^{-1}$), 635 nm ($\varepsilon = 70900\ M^{-1}cm^{-1}$) and 648 nm ($\varepsilon = 58100\ M^{-1}cm^{-1}$), respectively, which are more like the typical *p*-band of a closed-shell polycyclic aromatic hydrocarbon (PAH).[44] The optical energy-gaps (E_g^{opt}) of **BPT 1**, **BPT 2** and **CA 1** were estimated to be 1.09, 1.50 and 1.26 eV, respectively, based on their lowest energy absorption onset,[45] which are significantly narrow.[46] In contrast, the E_g^{opt} of **CA 2**, **CA 3**, and **CA 4** were determined to be 1.91, 1.90 and 1.80 eV, respectively. Moreover, **CA 2**, **CA 3** and **CA 4** exhibited intense emissions (Figure 3b) at 639, 643, and 674 nm, respectively. The relatively smaller stocks shifts of 9, 8 and 26 nm for **CA 2**, **CA 3** and **CA 4**, respectively, are implied to their structural rigidity[47] and weak π–π stacking capability of the **CA** cores due to the presence of bulky groups at the zigzag edge peripheries. Noteworthy, moderate fluorescence quantum yields (Φ_f) of 17–29% were estimated for **CA 2**, **CA 3** and **CA 4** (Table 1) in dilute solutions using rhodamine 6 g as reference; whereas compounds **BPT 1**, **BPT 2** and **CA 1**, did not show emissions in this range, which is consistent with the previously reported open-shell polycyclic hydrocarbons.[11,27]

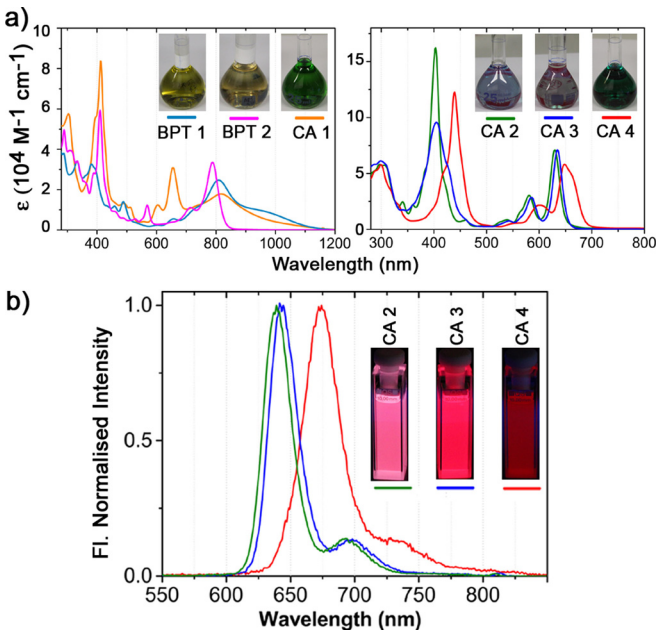

Figure 3. a) UV/Vis absorption (1×10^{-5} M) and b) emission spectra (1×10^{-6} M) of **BPTs** and **CAs** (**BPT 1**, **BPT 2**, **CA 2** and **CA 3** in CH_2Cl_2; **CA 1** and **CA 4** in $C_2H_2Cl_4$). The excitation wavelengths (λ_{ex}) for the fluorescent measurements were 403, 405, and 439 nm for **CA 2**, **CA 3** and **CA 4**, respectively. Inset photographs are taken under a) daylight and b) upon irradiation with a hand-held UV lamp.

The electrochemical properties of **BPTs** and **CAs** (Figure 4) were investigated by cyclic voltammetry (CV) in dry DCM, in which Ag/AgCl was used as the reference electrode. Due to the presence of $(CO\text{-}CCl)_2$ moiety, **BPT 1** and **CA 1** are highly electron deficient and display three reduction (E_{red}^{1-3}) waves (reversible and quasi-reversible) between −0.45 and −1.40 V, while **BPT 2** is moderately electron deficient and shows two reduction waves at −0.85 V (E_{red}^{1}) and −1.30 V (E_{red}^{2}). In addition, two oxidation waves (reversible and quasi-reversible) are observed for **BPT 1**, **BPT 2** and **CA 1** (E_{ox}^{1-2}) between 0.45 and 1.45 V. The electrochemical energy-gaps (E_g^{EC}) of **BPT 1**, **BPT 2** and **CA 1** are determined as 1.13, 1.47 and 1.33 eV, respectively, which are in accordance with their E_g^{opt}. The closed-shell **CA**

Table 1. Electrochemical and optical data of **BPTs** and **CAs**.[a]

	λ_{abs} [nm]	E^1_{red} [V]	E^2_{red} [V]	E^3_{red} [V]	E^1_{ox} [V]	E^2_{red} [V]	HOMO [eV]	LUMO [eV]	E_g^{opt}/E_g^{EC} [eV]
BPT 1	333, 381, 488, 809, 920 (br)	−0.55	−1.00	−1.29	0.58	1.10	−4.98	−3.85	1.09/1.13
BPT 2	410, 568, 788	−0.85	−1.30	–	0.62	1.14	−5.02	−3.55	1.50/1.47
CA 1	412, 655, 816 (br)	−0.48	−0.99	−1.31	0.85	1.36	−5.25	−3.92	1.26/1.33
CA 2	403, 581, 630	−1.07	−1.47	–	0.76	1.34	−5.16	−3.33	1.91/1.83
CA 3	405, 586, 635	−1.09	−1.47	–	0.75	1.31	−5.15	−3.31	1.90/1.84
CA 4	439, 601, 648	−0.87	−1.31	–	0.89	1.40	−5.29	−3.53	1.80/1.76

[a] E^{1-3}_{red} and E^{1-2}_{ox} are half-wave potentials of the reductive and oxidative waves (vs. Ag/AgCl), respectively. The HOMO/LUMO are determined by the equation: HOMO/LUMO = −(4.4 + $E^1_{ox/red}$) eV.

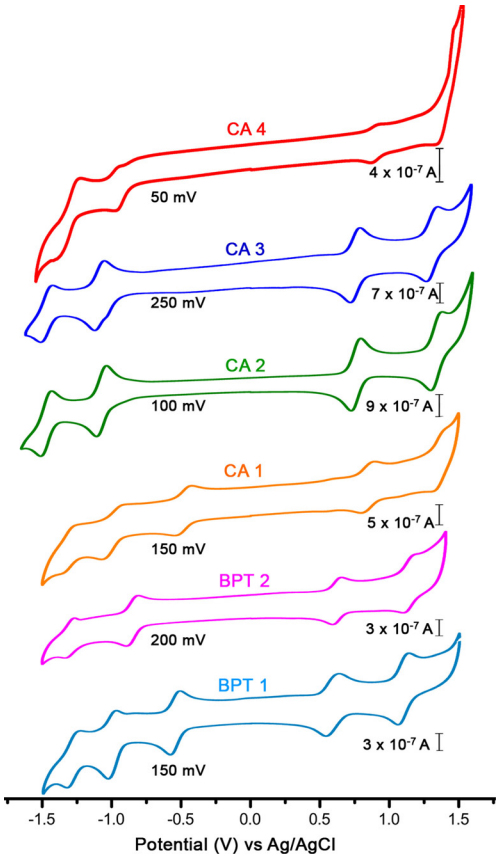

Figure 4. Cyclic voltammetry of **BPTs** and **CAs** in dry DCM with 0.1 M Bu_4NPF_6 as the supporting electrolyte, Ag/AgCl as reference electrode, Pt disk as working electrode, and Pt wire as counter electrode. Scan rate used is 50–250 mV.

2, **CA 3** and **CA 4** reveal two reduction waves and two oxidation waves, and their corresponding E_g^{opt} are estimated to be 1.83, 1.84 and 1.76 eV, respectively. All the optical and electrochemical properties of **BPTs** and **CAs** are summarized in Table 1.

Conclusions

In summary, we demonstrated the novel modulation of magnetic properties of zigzag-edged NGs via the controlled Diels–Alder reaction with **4-PA**. Accordingly, the unstable open-shell **4-PA** ($y_0 = 0.72$) biradicaloid was converted into stable open-shell **BPT 1** and **BPT 2** (**BPT 1**, $y_0 = 0.55$; **BPT 2**, $y_0 = 0.61$) upon respective one-side Diels–Alder reaction. A step-wise Diels–Alder reaction was carried out with **4-PA** and, hence, achieving the open-shell **CA 1** ($y_0 = 0.46$) with asymmetric edge-substitutions. Notably, **BPT 1**, **BPT 2** and **CA 1** biradicaloids possessed narrow energy gaps (≈1.1–1.5 eV) and exhibited remarkable stability under ambient conditions. On the other hand, the two-fold Diels–Alder reaction of **4-PA** with suitable dienophiles gave closed-shell **CA 2**, **CA 3** and **CA 4**. Our synthetic strategy reported herein shed light on the development of open-shell zigzag-edged NGs with tailor-made magnetic properties with high stability, which can be useful for the advancement of carbon-based nanomaterials with superior quantum performance capability.[20,21]

Experimental Section

Synthesis of PA 1

Compound **PA 1** was synthesized by following the previous report.[28]

Synthesis of BPT 1

A Schlenk flask was charged with **PA 1** (55.0 mg, 0.058 mmol), and *p*-chloranil (28.4 mg, 0.116 mmol) along with dry toluene (10 mL) under argon. The flask was placed in a preheated oil bath at 105 °C and magnetically stirred for 24 h. The solution brought to RT and the solvent was removed in vacuo. The crude solid was purified by silica gel column chromatography with DCM/*iso*-hexane mixture as eluent to afford **BPT 1**, along with its monochloro derivative, as dark greenish yellow solid. The minor monochloro **BPT 1** impurity is inseparable and the combined yield is 40% (26 mg). $R_f = 0.55$ (*iso*-hexane/DCM 1:1 *v/v*). ^{1}H NMR (500 MHz, $C_2D_2Cl_4$, 60 °C): $\delta =$ 9.43 (d, 10.2, 1H), 9.34 (d, 10.2, 1H), 9.08 (d, 7.6, 2H), 7.93 (t, 7.5, 2H), 7.8–7.7 (2H), 7.68 (d, 10.2, 1H), 7.64 (d, 10.2, 1H), 7.21 (d, 10.2, 2H), 7.19 (d, 10.2, 2H), 7.09 (d, 10.2, 2H), 7.06 (d, 10.2, 2H), 6.73 (2 *x* s, 4H), 2.37 (s, 6H), 1.87 (s, 6H), 1.79 (s, 6H), 1.47 (s, 9H), 1.46 ppm (s, 9H). ^{13}C NMR (125 MHz, $C_2D_2Cl_4$, 60 °C): $\delta = 178.0$, 149.2, 149.0, 143.0, 142.9, 141.3, 140.5, 139.8, 136–137, 132.4, 132.0, 131.8, 131.4, 131.0, 130.4, 129.0, 128.9, 128.2, 128.1, 128.0, 127.7, 127.3, 127.1, 126.6, 126.4, 125.6, 125.1, 125.0, 124.5, 123.5, 122.8, 122.3, 121.8, 34.2, 31.3, 21.0, 20.9 ppm. Detailed ^{1}H and ^{13}C signal assignments are given in Table S3. HR-MS MALDI (*m/z*): calcd for $C_{80}H_{58}Cl_2O_2$ $[M]^+$, 1120.381; found, 1120.385.

Synthesis of BPT 2

Compound **PA 1** (53.5 mg, 0.056 mmol), and DDQ (25.5 mg, 0.113 mmol) along with dry DCM (6 mL) were charged in a dry 25 mL Schlenk tube and stirred at RT for 24 h under argon. The solvent was removed in vacuo and the crude solid was purified by silica gel column chromatography with DCM as eluent to afford **BPT 2** (11.5 mg, 20%) as dark-brown solid. $R_f = 0.61$ (DCM). ^{1}H NMR (500 MHz, $C_2D_2Cl_4$, 60 °C): δ 9.06 (d, 7.4, 2H), 8.23 and 8.22 (2 *x* d, 9.7, 4H), 7.91 (2H), 7.73–7.65 (3H), 7.60 (d, 9.7, 1H), 7.20 (d, 8.5, 2H), 7.18 (d, 8.5, 2H), 7.05 (d, 8.5, 2H), 7.03 (d, 8.5, 2H), 6.73 (s, 2H), 6.72 (s, 2H), 2.36 (s, 6H), 1.86 (s, 6H), 1.77 (s, 6H), 1.46 and 1.45 ppm (2×s, 18H) ppm. ^{13}C NMR (125 MHz, $C_2D_2Cl_4$, 60 °C): δ = 149.2, 149.1, 141.4, 140.6, 140.0, 139.4, 137.2, 136.7, 136.6, 136.5, 136.4, 136.3, 136.0, 133.8, 132.7, 132.6, 132.1, 132.0, 131.9, 131.4, 131.1, 130.9, 130.8, 129.4, 129.0, 128.8, 128.3, 128.2, 127.7, 127.2, 126.6, 126.2, 125.5, 125.3, 125.1, 124.8, 124.1, 123.9, 123.7, 123.6, 123.5, 122.9, 122.7, 122.2, 121.8, 121.6, 116.3, 106.4, 34.2, 31.3, 21.0, 20.9, 20.8 ppm. Detailed ^{1}H and ^{13}C signal assignments are given in Table S3. HR-MS MALDI (*m/z*): calcd for $C_{78}H_{58}N_2$ $[M]^+$, 1022.460; found, 1022.466.

Synthesis of CA 1

A solution of **BPT 1** (10.5 mg, 0.009 mmol), diethyl acetylenedicarboxylate (**3**) (477.6 mg, 2.81 mmol), and *p*-chloranil (6.9 mg, 0.028 mmol) in dry toluene (4 mL) was heated at 105 °C with gentle stirring under argon. After 24 h, excess of *p*-chloranil (20.0 mg) was added to the reaction mixture and continued heating for 2 h. The solvent was removed in vacuo and the crude solid was purified by silica gel column chromatography with DCM as eluent to afford **CA 1** (3 mg, 25%) as dark-green solid. $R_f = 0.63$ (DCM). ^{1}H NMR (500 MHz, $C_2D_2Cl_4$, 60 °C): δ = 10.13 (d, 10.1, 1H), 9.97 (d, 10.0, 1H), 9.21 (d, 9.5, 1H), 8.67 (d, 9.5, 1H), 8.58 (d, 10.1, 1H), 8.55 (d, 10.0, 1H), 8.67 (d, 9.5, 1H), 8.60 (d, 9.5, 1H), 7.45 (d, 7.9, 2H), 7.42–7.32 (6H), 6.91 (s, 2H), 6.89 (s, 2H), 4.79 and 4.77 (2 *x* q, 7.2, 4H), 2.50 (s, 6H), 1.82 (s, 6H), 1.79 (s, 6H), 1.64 and 1.62 (2 *x* t, 7.2, 6H), 1.60 (s, 9H), 1.58 ppm (s, 9H). ^{13}C NMR (125 MHz, $C_2D_2Cl_4$, 60 °C): δ = 179.0, 168.7, 168.5, 149.5, 149.4, 143.1, 142.9, 140.3, 139.5, 139.4, 138.8, 137.9, 137.7, 137.3, 137.1, 137.0, 136.9, 136.8, 132.2, 131.1, 131.0, 130.4, 129.7, 129.6, 129.2, 129.0, 128.9, 128.6, 128.4, 128.3, 128.1, 128.0, 127.5, 127.3, 127.2, 126.4, 125.9, 125.6, 125.5, 125.1, 123.6, 123.5, 123.4, 122.9, 122.1, 122.0, 121.7, 121.6, 121.3, 120.9, 120.6, 120.3, 119.8, 119.7, 119.5, 62.4, 62.3, 34.3, 31.5, 31.4, 21.3, 21.2, 14.2 ppm. Detailed ^{1}H and ^{13}C signal assignments are given in Table S3. HR-MS MALDI (*m/z*): calcd for $C_{88}H_{66}Cl_2O_6$ $[M]^+$, 1288.424; found, 1288.428.

Synthesis of CA 2

A Schlenk flask was charged with **PA 1** (50.0 mg, 0.053 mmol), **3** (470.7 mg, 2.63 mmol), and *p*-chloranil (32.3 mg, 0.131 mmol) along with dry toluene (10 mL) under argon. The solution was heated at 105 °C and magnetically stirred for 20 h. The resultant dark brown solution was mixed with excess of *p*-chloranil (80.0 mg) and heated for another 4 h. The solution brought to RT and the solvent was removed in vacuo. The crude solid purified by silica gel column chromatography with DCM as eluent to afford **CA 2** (21.6 mg, 32%) as purplish green solid. $R_f = 0.21$ (DCM). ^{1}H NMR (500 MHz, CD_2Cl_2, 30 °C): δ = 9.11 (d, 9.7, 2H), 9.10 (d, 9.7, 2H), 8.55 (d, 9.7, 2H), 8.50 (d, 9.7, 2H), 7.35 (8.3, 8H), 6.89 (s, 4H), 4.73 and 4.72 (2 *x* q, 7.2, 8H), 1.77 (s, 12H), 1.58 and 1.59 (2 *x* t, 7.2, 12H), 1.54 (s, 18H), 2.46 (s, 6H) ppm. ^{13}C NMR (125 MHz, CD_2Cl_2, 30 °C): δ 169.3, 169.2, 149.7, 139.0, 138.8, 138.2, 137.6, 137.2, 131.2, 130.2, 129.8, 129.6, 128.8, 128.4, 127.5, 127.3, 127.2, 126.0, 125.9, 125.7, 125.3, 124.1, 122.1, 122.0, 121.8, 121.6, 120.7, 120.5, 120.3, 62.8, 34.8, 31.7, 21.5, 14.5 ppm. Detailed ^{1}H and ^{13}C signal assignments are given in Table S4. HR-MS MALDI (*m/z*): calcd for $C_{90}H_{76}O_8$ $[M]^+$, 1284.554; found, 1284.558.

Synthesis of CA 3

A mixture of **PA 1** (31.0 mg, 0.033 mmol), 1,4-diphenyl-2-butyne-1,4-dione (**4**) (224.0 mg, 0.912 mmol), and *p*-chloranil (20.0 mg, 0.081 mmol) in dry toluene (6 mL) was heated at 105 °C with stirring under argon. After 24 h, the resultant dark brown solution was mixed with excess of *p*-chloranil (50.0 mg) and heated for another 4 h. The solvent was removed in vacuo and the solid was purified by silica gel column chromatography with DCM as eluent to afford **CA 3** (13.8 mg, 30%) as dark green solid. $R_f = 0.37$ (DCM). ^{1}H NMR (500 MHz, $C_2D_2Cl_4$, 30 °C): δ = 8.53 (d, 9.6, 4H), 8.40 (d, 9.6, 2H), 8.31 (d, 9.6, 2H), 7.87 and 7.84 (2×d, 8.0, 8H), 7.58 (4H), 7.40 and 7.38 (2 *x* t, 8.0, 8H), 7.28 (d, 7.9, 4H), 7.24 (d, 7.9, 4H), 6.79 (s, 4H), 2.39 (s, 6H), 1.74 (s, 12H), 1.46 (s, 18H) ppm. ^{13}C NMR (125 MHz, $C_2D_2Cl_4$, 30 °C): δ = 199.5, 199.3, 149.0, 138.5, 138.0, 137.6, 137.3, 136.9, 136.5, 133.7, 133.1, 133.0, 130.5, 130.3, 129.5, 129.0, 128.9, 128.5, 128.2, 127.6, 126.9, 125.9, 125.7, 125.4, 125.1, 123.5, 121.5, 121.1, 121.0, 120.9, 120.3, 120.1, 119.9, 34.2, 31.4, 21.2 ppm. Detailed ^{1}H and ^{13}C signal assignments are given in Table S4. HR-MS MALDI (*m/z*): calcd for $C_{106}H_{76}O_4$ $[M]^+$, 1412.574; found, 1412.568.

Synthesis of CA 4

Compound **PA 1** (7.0 mg, 0.007 mmol), *N*-phenylmaleimide (**5**) (63.7 mg, 0.367 mmol), and *p*-chloranil (4.5 mg, 0.018 mmol) were mixed with dry toluene (3 mL) and heated at 105 °C with stirring under argon. After 24 h, excess of *p*-chloranil (20.0 mg) was added to the reaction tube and continued the heating for another 4 h. The solvent was removed in vacuo and solid was purified by silica gel column chromatography with DCM as eluent to afford **CA 4** (3.0 mg, 31%) as dark green solid. $R_f = 0.36$ (DCM). ^{1}H NMR (500 MHz, $C_2D_2Cl_4$, 60 °C): δ = 10.09 (d, 9.2, 2H), 10.07 (d, 9.2, 2H), 8.77 (d, 9.2, 2H), 8.74 (d, 9.2, 2H), 7.78 (d, 7.8, 4H), 7.68 (t, 7.8, 4H), 7.56 (t, 7.8, 2H), 7.38 (s, 8H), 6.93 (s, 4H), 2.52 (s, 6H), 1.82 (s, 12H), 1.58 ppm (s, 18H). No ^{13}C NMR data due to low solubility. Detailed ^{1}H signal assignments are given in Table S4. HR-MS MALDI (*m/z*): calcd for $C_{94}H_{66}N_2O_4$ $[M]^+$, 1286.502; found, 1286.498.

Acknowledgements

This work was financially supported by the European Union's Horizon 2020 research and innovation programme under grant agreement No. 785219, EU Graphene Flagship, the German Research Foundation (DFG) within the Cluster of Excellence "Center for Advancing Electronics Dresden (cfaed)" and EnhanceNano (No. 391979941) as well as the European Social Fund and the Federal State of Saxony (ESF-Project "GRAPHD", TU Dresden). The authors acknowledge the use of computational facilities at the Center for information services and high performance computing (ZIH) at TU Dresden. Diffraction data have been collected on BL14.3 at the BESSY II electron storage ring operated by the Helmholtz-Zentrum Berlin; we would particularly like to acknowledge the help and support of Manfred Weiss and his group members during the experiments at BESSY II. We thank Dr. Tilo Lübken (Organic Chemistry, Techni-

sche Universität Dresden) for additional NMR analyses. We thank Prof. Dr Martin Baumgarten (Max Planck Institute for Polymer Research, Germany) for the EPR measurements. J.L. is grateful for the startup funding from The University of Hong Kong and the funding support from ITC to the SKL. Open access funding enabled and organized by Projekt DEAL.

Conflict of interest

The authors declare no conflict of interest.

Keywords: circumacenes · Diels–Alder reaction · *peri*-acenes · singlet biradicals · zigzag edges

[1] A. Narita, X.-Y. Wang, X. Feng, K. Müllen, *Chem. Soc. Rev.* **2015**, *44*, 6616 – 6643.
[2] J. Cai, P. Ruffieux, R. Jaafar, M. Bieri, T. Braun, S. Blankenburg, M. Muoth, A. P. Seitsonen, M. Saleh, X. Feng, K. Müllen, R. Fasel, *Nature* **2010**, *466*, 470 – 473.
[3] J. Wu, W. Pisula, K. Müllen, *Chem. Rev.* **2007**, *107*, 718 – 747.
[4] E. Clar, *Polycyclic Hydrocarbons*, Vols. 1, 2, Academic Press, London, **1964**.
[5] X.-Y. Wang, A. Narita, K. Müllen, *Nat. Rev. Chem.* **2017**, *1*, 0100.
[6] A. Narita, Z. Chen, Q. Chen, K. Müllen, *Chem. Sci.* **2019**, *10*, 964 – 975.
[7] M. Burghard, H. Klauk, K. Kern, *Adv. Mater.* **2009**, *21*, 2586 – 2600.
[8] L. Chen, Y. Hernandez, X. Feng, K. Müllen, *Angew. Chem. Int. Ed.* **2012**, *51*, 7640 – 7654; *Angew. Chem.* **2012**, *124*, 7758 – 7773.
[9] G. Z. Magda, X. Jin, I. Hagymási, P. Vancsó, Z. Osváth, P. Nemes-Incze, C. Hwang, L. P. Biró, L. Tapasztó, *Nature* **2014**, *514*, 608 – 611.
[10] J. Hu, X. Ruan, Y. P. Chen, *Nano Lett.* **2009**, *9*, 2730 – 2735.
[11] J. Ma, J. Liu, M. Baumgarten, Y. Fu, Y. Z. Tan, K. S. Schellhammer, F. Ortmann, G. Cuniberti, H. Komber, R. Berger, K. Mullen, X. Feng, *Angew. Chem. Int. Ed.* **2017**, *56*, 3280 – 3284; *Angew. Chem.* **2017**, *129*, 3328 – 3332.
[12] J. Ma, K. Zhang, K. S. Schellhammer, Y. Fu, H. Komber, C. Xu, A. A. Popov, F. Hennersdorf, J. J. Weigand, S. Zhou, W. Pisula, F. Ortmann, R. Berger, J. Liu, X. Feng, *Chem. Sci.* **2019**, *10*, 4025 – 4031.
[13] G. E. Rudebusch, J. L. Zafra, K. Jorner, K. Fukuda, J. L. Marshall, I. Arrechea-Marcos, G. L. Espejo, R. P. Ortiz, C. J. Gómez-García, L. N. Zakharov, M. Nakano, H. Ottosson, J. Casado, M. M. Haley, *Nat. Chem.* **2016**, *8*, 753 – 759.
[14] R. Rausch, D. Schmidt, D. Bialas, I. Krummenacher, H. Braunschweig, F. Würthner, *Chem. Eur. J.* **2018**, *24*, 3420 – 3424.
[15] Z. Sun, Q. Ye, C. Chi, J. Wu, *Chem. Soc. Rev.* **2012**, *41*, 7857 – 7889.
[16] Q. Ye, C. Chi, *Chem. Mater.* **2014**, *26*, 4046 – 4056.
[17] Z. Sun, Z. Zeng, J. Wu, *Acc. Chem. Res.* **2014**, *47*, 2582 – 2591.
[18] D. Lungerich, O. Papaianina, M. Feofanov, J. Liu, M. Devarajulu, S. I. Troyanov, S. Maier, K. Amsharov, *Nat. Commun.* **2018**, *9*, 4756.
[19] A. Konishi, Y. Hirao, K. Matsumoto, H. Kurata, R. Kishi, Y. Shigeta, M. Nakano, K. Tokunaga, K. Kamada, T. Kubo, *J. Am. Chem. Soc.* **2013**, *135*, 1430 – 1437.
[20] F. Lombardi, A. Lodi, J. Ma, J. Liu, M. Slota, A. Narita, W. K. Myers, K. Müllen, X. Feng, L. Bogani, *Science* **2019**, *366*, 1107 – 1110.
[21] M. Slota, A. Keerthi, W. K. Myers, E. Tretyakov, M. Baumgarten, A. Ardavan, H. Sadeghi, C. J. Lambert, A. Narita, K. Müllen, L. Bogani, *Nature* **2018**, *557*, 691 – 695.
[22] J. Li, S. Sanz, M. Corso, D. J. Choi, D. Peña, T. Frederiksen, J. I. Pascual, *Nat. Commun.* **2019**, *10*, 200.
[23] O. V. Yazyev, M. I. Katsnelson, *Phys. Rev. Lett.* **2008**, *100*, 047209.
[24] M. Nakano, R. Kishi, S. Ohta, H. Takahashi, T. Kubo, K. Kamada, K. Ohta, E. Botek, B. Champagne, *Phys. Rev. Lett.* **2007**, *99*, 033001.
[25] A. Konishi, Y. Hirao, M. Nakano, A. Shimizu, E. Botek, B. Champagne, D. Shiomi, K. Sato, T. Takui, K. Matsumoto, H. Kurata, T. Kubo, *J. Am. Chem. Soc.* **2010**, *132*, 11021 – 11023.
[26] Y. Li, K.-W. Huang, Z. Sun, R. D. Webster, Z. Zeng, W. Zeng, C. Chi, K. Furukawa, J. Wu, *Chem. Sci.* **2014**, *5*, 1908 – 1914.
[27] J. Liu, P. Ravat, M. Wagner, M. Baumgarten, X. Feng, K. Müllen, *Angew. Chem. Int. Ed.* **2015**, *54*, 12442 – 12446; *Angew. Chem.* **2015**, *127*, 12619 – 12623.
[28] M. R. Ajayakumar, Y. Fu, J. Ma, F. Hennersdorf, H. Komber, J. J. Weigand, A. Alfonsov, A. A. Popov, R. Berger, J. Liu, K. Müllen, X. Feng, *J. Am. Chem. Soc.* **2018**, *140*, 6240 – 6244.
[29] Y. Ni, T. Y. Gopalakrishna, H. Phan, T. S. Herng, S. Wu, Y. Han, J. Ding, J. Wu, *Angew. Chem. Int. Ed.* **2018**, *57*, 9697 – 9701; *Angew. Chem.* **2018**, *130*, 9845 – 9849.
[30] S. Mishra, T. G. Lohr, C. A. Pignedoli, J. Liu, R. Berger, J. Urgel, K. Müllen, X. Feng, P. Ruffieux, R. Fasel, *ACS Nano* **2018**, *12*, 11917 – 11927.
[31] S. Yamanaka, M. Okumura, M. Nakano, K. Yamaguchi, *J. Mol. Struct. Theochem.* **1994**, *310*, 205 – 218.
[32] R. Berger, M. Wagner, X. Feng, K. Müllen, *Chem. Sci.* **2015**, *6*, 436 – 441.
[33] E. H. Fort, P. M. Donovan, L. T. Scott, *J. Am. Chem. Soc.* **2009**, *131*, 16006 – 16007.
[34] E. H. Fort, L. T. Scott, *Angew. Chem. Int. Ed.* **2010**, *49*, 6626 – 6628; *Angew. Chem.* **2010**, *122*, 6776 – 6778.
[35] G. Trinquier, J.-P. Malrieu, *J. Phys. Chem. A* **2018**, *122*, 1088 – 1103.
[36] J.-P. Malrieu, G. Trinquier, *J. Phys. Chem. A* **2016**, *120*, 9564 – 9578.
[37] R. D. Broene, F. Diederich, *Tetrahedron Lett.* **1991**, *32*, 5227 – 5230.
[38] D.-e. Jiang, S. Dai, *Chem. Phys. Lett.* **2008**, *466*, 72 – 75.
[39] Z. Jia, K. Nakajima, K.-i. Kanno, Z. Song, T. Takahashi, *ChemistrySelect* **2018**, *3*, 4298 – 4302.
[40] G. London, M. von Wantoch Rekowski, O. Dumele, W. B. Schweizer, J.-P. Gisselbrecht, C. Boudon, F. Diederich, *Chem. Sci.* **2014**, *5*, 965 – 972.
[41] W.-L. Xu, H. Zhang, Y.-L. Hu, H. Yang, J. Chen, L. Zhou, *Org. Lett.* **2018**, *20*, 5774 – 5778.
[42] B. Bleaney, K. D. Bowers, *Proc. R. Soc. London, Ser. A* **1952**, *214*, 451 – 465.
[43] D. Geuenich, K. Hess, F. Köhler, R. Herges, *Chem. Rev.* **2005**, *105*, 3758 – 3772.
[44] E. Clar, J. M. Robertson, R. Schlogl, W. Schmidt, *J. Am. Chem. Soc.* **1981**, *103*, 1320 – 1328.
[45] J. Li, C. Jiao, K.-W. Huang, J. Wu, *Chem. Eur. J.* **2011**, *17*, 14672 – 14680.
[46] D. Jänsch, I. Ivanov, Y. Zagranyarski, I. Duznovic, M. Baumgarten, D. Turchinovich, C. Li, M. Bonn, K. Müllen, *Chem. Eur. J.* **2017**, *23*, 4870 – 4875.
[47] J. Lee, H. Li, A. J. Kalin, T. Yuan, C. Wang, T. Olson, H. Li, L. Fang, *Angew. Chem. Int. Ed.* **2017**, *56*, 13727 – 13731; *Angew. Chem.* **2017**, *129*, 13915 – 13919.

Manuscript received: March 4, 2020
Revised manuscript received: April 11, 2020
Accepted manuscript online: April 16, 2020
Version of record online: May 12, 2020

